NANO LETTERS

pubs.acs.org/NanoLett Letter

PNP Nanofluidic Transistor with Actively Tunable Current Response and Ionic Signal Amplification

Yu-Lin Hu,[‖] Yu Hua,[‖] Zhong-Qin Pan, Jia-Han Qian, Xiao-Yang Yu, Ning Bao, Xiao-Lei Huo,* Zeng-Qiang Wu,* and Xing-Hua Xia*

Cite This: *Nano Lett.* 2022, 22, 3678−3684 Read Online

ACCESS | Metrics & More | Article Recommendations | Supporting Information

ABSTRACT: Inspired by electronic transistors, electric field gating has been adopted to manipulate ionic currents of smart nanofluidic devices. Here, we report a PNP nanofluidic bipolar junction transistor (nBJT) consisting of one polyaniline (PANI) layer sandwiched between two polyethylene terephthalate (PET) nanoporous membranes. The PNP nBJT exhibits three different responses of currents (quasi-linear, rectification, and sigmoid) due to the counterbalance between surface charge distribution and base voltage applied in the nanofluidic channels; thus, they can be switched by base voltage. Four operating modes (cutoff, active, saturation, and breakdown mode) occur in the collector response currents. Under optimal conditions, the PNP nBJT exhibits an average current gain of up to 95 in 100 mM KCl solution at a low base voltage of 0.2 V. The present nBJT is promising for fabrication of nanofluidic devices with logical-control functions for analysis of single molecules.

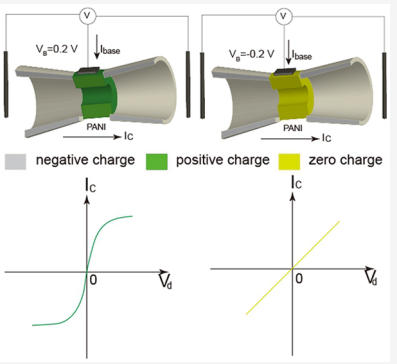

KEYWORDS: *nanofluidic bipolar junction transistor, PNP, ion transport, iontronics, current amplification*

Recent applications of nanofluidic devices, such as nanochannels and nanopores, have been extended from the detection of single molecules[1,2] to the regulation of ion transport.[3,4] Transport of ions in nanoconfined environments exhibits unique properties compared with those in bulk environments because of the remarkable influence of surface charge and van der Waals (vdW).[5] In addition, the interactions of ions and molecules occurring in nanoscale spaces will considerably affect their movement,[6] which might be used to replace solid-state electronics in mimicking signal transmission and treatment in biology.

In nanofluidic devices, selective ion transport occurs due to the presence of electric potential gradient at the surface of nanochannel, generating a phenomenon of ion current rectification (ICR). High ICR ratio in nanofluidic diodes could be achieved through optimization of geometry,[7,8] surface charges distribution,[9,10] and/or concentration profiles.[11] For instance, serial and parallel connections of nanofluidic diodes in circuits have been proposed for achieving high ICR ratio and logic control by referring the structure of integrated circuits (ICs).[12,13] Although a combination of nanochannels and other circuit units makes the nanofluidics feasible to deal with signal transduction[14−16] and energy conversion,[17] these proposed devices could only passively respond to the change of external conditions.[3,4,18−20] Thus, they have to be designed according to specific environments but they are hardly adaptable to environmental changes. To address this issue, Reed's group proposed an actively modulated nanofluidic diode by implanting the concept of field effect transistors (FET), which allows the modulation of the surface charge distribution of nanochannels using gate voltage,[21] implying the possibility of actively manipulating the transportation of molecules in nanofluidic channels. Recently, nanofluidic FET (nFET) have also been successfully utilized in nanocapillaries to reduce the velocity of DNA translocation and improve the signal-to-noise ratio.[22]

Conventional ICs diodes and transistors fabricated with semiconductors have been successfully used for accurate manipulation and amplification of electric signals. From this point of view, nanofluidic channels with the ICR functions could be regarded as ionic components to construct ionic devices with current-amplification functions for analysis in solutions. Up to date, a few ionic devices for current amplification in solutions have been proposed. Berggren et al. reported an ionic bipolar transistor in microchips consisting of ionic gels with different charges, achieving high ionic signal outputs at a gain of 10 under a voltage of 4 V across the emitter and base terminal.[23] Chang et al. also reported a ionic device by integrating an anion exchange membrane in a microfluidic device with a ionic current gain of 45 under a

Received: January 24, 2022
Revised: April 14, 2022
Published: April 20, 2022

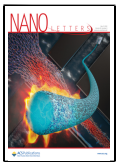

https://doi.org/10.1021/acs.nanolett.2c00312
Nano Lett. 2022, 22, 3678−3684

voltage of 20 V across the input fluidic channel.[24] Since a large part of the applied voltage need to maintain the cationic selectivity of the film, only a small portion of the voltage could be applied on driving ions across the bipolar junction transistors, leading to a much lower current amplification ratio.

Here, we propose to integrate the concept of transistors nanofluidic device to fabricate a PNP nBJT consisting of one polyaniline (PANI) layer sandwiched between two polyethylene terephthalate (PET) nanoporous membranes as schematically illustrated in Scheme 1. In this device, the base voltage and driving voltage can be applied on the PANI layer and across the nBJT, respectively. Since the surface charges of PANI (positively charged in oxidized state)[25−27] and PET (negatively charged) are different,[28] the nBJT can be defined as a PNP nBJT. We then studied the influence of base voltage on the current responses of the PNP nBJT. Instead of choosing electrons and holes as the charge carriers in solid-state electronics, cations and anions as the charge carriers in nanofluidic devices could mimic the information transmission of biological system.[29]

Scheme 1. Schematic Illustration of the PNP nBJT Working Principle and Experimental Setup[a]

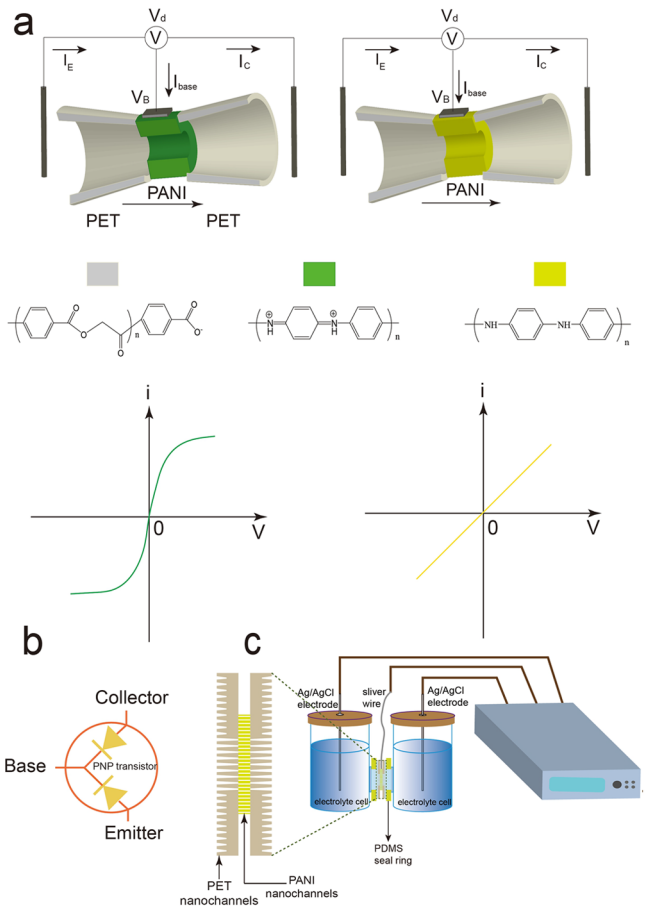

[a](a) One PANI membrane is sandwiched between two PET nanochannels to build a PNP nBJT; A driving voltage (V_d) is applied by two Ag/AgCl electrodes. A silver wire is connected to the PANI membrane to provide a base voltage (V_B). When the applied V_B is high enough to convert the PANI layer into its oxidizing state (green) carrying positive charges, a sigmoid $I-V$ curve occurs. While the applied V_B is lower than the oxidation potential of PANI, PANI will be converted to its reducing state (yellow) carrying zero charge, a quasi-linear curve will be observed. I_{base}, current in PANI region; I_E and I_C, currents through PET nanochannels of the PNP nBJT. (b) Corresponding circuit symbols of the PNP nBJT. (c) Experimental setup of the PNP nBJT. A PNP nBJT is mounted between two homemade electrolyte cells filled with electrolytes. The enlarged region describes how the PNP nBJT is connected with the experimental instruments. A bipotentiostat is used to apply V_d and V_B, respectively, and record ionic currents passing through the PNP nBJT by two Ag/AgCl reference electrodes.

RESULTS AND DISCUSSION

The assembled PNP nBJT by inserting a PANI membrane carrying positive charges into two PET nanochannels with negative charges is illustrated in Scheme S1 (Supporting Information). The seamless integration makes the device possible to fully apply the voltage on driving ions across the junctions, thus the output current could be significantly amplified as compared to the reported ones.[23]

Figure 1a,b illustrates the typical SEM images of the base side of a PET nanoporous membrane and the PANI layer covered tip side of the PET membrane, respectively. Four conical structures with diameter of 220 nm in the base side are revealed by the enlarged SEM image as inset. The average size of the nanochannels at tip side is calculated to be around 130 nm based on the method in Supporting Information (Figure S2). The inset in Figure 1b displays a cross-sectional image of the PET membrane covered with a PANI layer of 5 μm in thickness. Figure 1c shows the Fourier transform infrared (FT-IR) spectra of the PET membrane and the deposited PANI layer. There are two peaks that appear at 1728 and 1265 cm^{-1}, which can be attributed to the stretching of C═O groups and C−C(O)−C groups in the PET membrane, respectively. The peaks at wavelengths of 1485 and 1582 cm^{-1} might be ascribed to the stretching vibrations of quinoid rings and benzenoid rings in PANI membrane, respectively. These results demonstrate that the PANI layer has been successfully modified on the surface of PET nanoporous membrane.

Figure 1d illustrates a current−voltage ($I-V$) curve measured on a native PET nanoporous membrane. It shows a feature for the cation-rectification responses of the PET membrane in 10 mM KCl solution with pH value of 6.5, since the PET nanoporus membrane carries negative charges in a solution with pH higher than the pK_a (which is about 3) of the carboxyl groups at PET surface. After the PANI membrane was coated at the tip side of the PET nanoporous membrane, the current response is reversed to anion rectification (Figure 1e). This could be ascribed to the positive charges appearing on surface of the PANI membrane at its oxidizing state. In addition, the PANI membrane modification increases the rectification ratio, which might be due to different distributions of surface charges and decreased size of the nanochannels upon PANI membrane coating.

PANI is a conductive polymer and can be reversibly switched between reducing and oxidizing states in a potential range from −0.2 to 0.6 V as displayed in the cyclic voltammogram (Figure S3). Since the surface charges of PANI can be electrochemically switched from neutral (reducing state)[26] to positive (oxidizing state), the ion transport can be easily regulated by applying base voltage on the PANI membrane. The thickness of the PANI membrane was controlled by polymerization time, which could be regulated from 1 (Figure S4) to 5 μm (Figure 1b, inset).

We found that the current responses (I_C-V) of the PNP nBJT varied under base voltage (V_B) in different regions. By

https://doi.org/10.1021/acs.nanolett.2c00312
Nano Lett. 2022, 22, 3678−3684

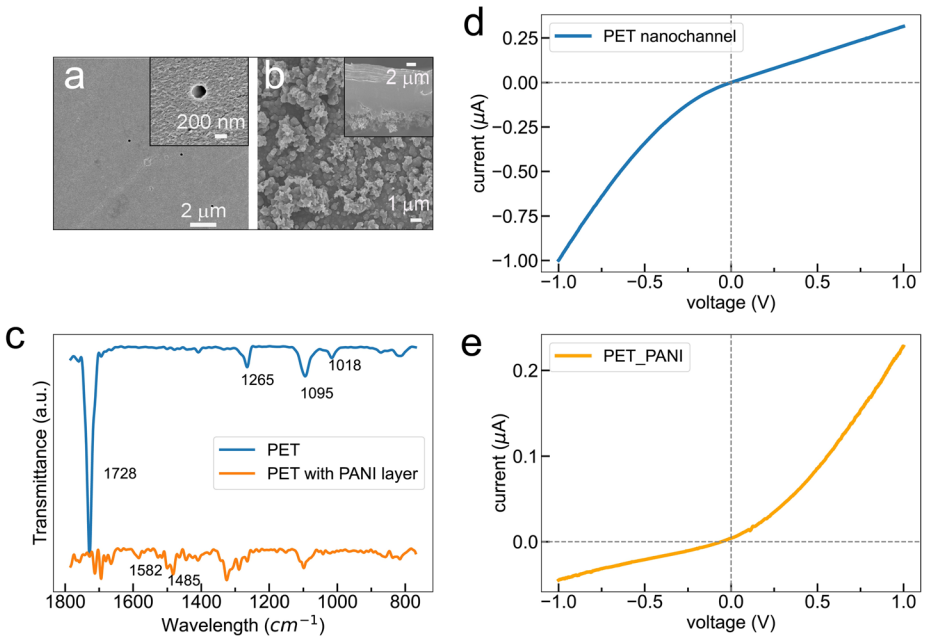

Figure 1. SEM images of PET sides with base opening (a) and PANI layer at the tip side of PET membrane (b). Inset shows the cross-sectional image of the PET membrane with a PANI layer of 5 μm in thickness. (c) FT-IR spectra of the PET and PANI layer coated PET layers. $I-V$ curves of the PET nanoporous membranes without (d) and with PANI coating layer (e) in 10 mM KCl.

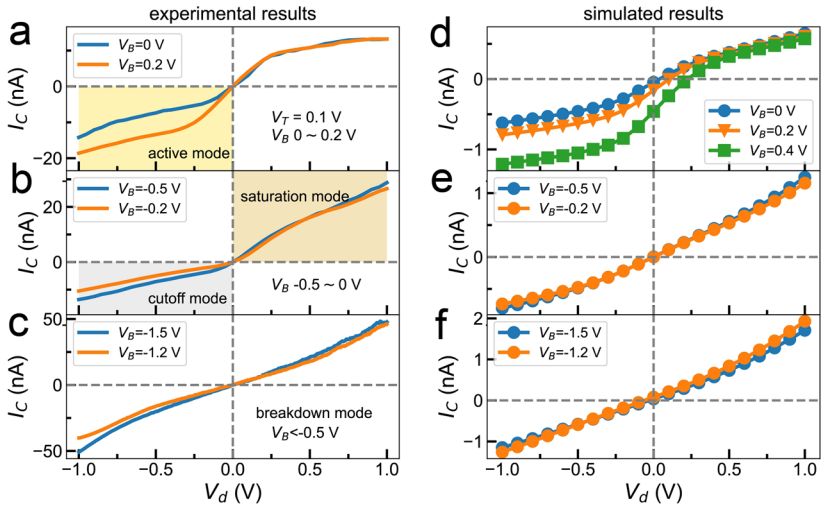

Figure 2. $I(I_C)-V$ curves of a PNP nBJT with different base voltages (V_B) in 10 mM KCl obtained from experimental measurements (left panel) and theoretical simulations (right panel). (a) Yellow region, active mode; (b) Gold region, saturation mode, gray region, cutoff mode; (c) Breakdown mode.

applying V_B to 0 and 0.2 V, a sigmoid (S-shape curve) I_C-V relationship appears, as revealed in Figure 2a. This might be ascribed because the PANI membrane starts to carry partially positive charges because the reducing state of the PANI layer could be converted to its oxidizing state at the applied base voltages. The threshold voltage of the PNP nBJT was investigated by measuring I_C at −1 V and V_B from −0.5 to 1.0 V. It could be observed that I_C increases at around 0.1 V (Figure S5, Supporting Information). Appearance of the sigmoid $I-V$ curve means that the ionic current (I_C) experiences a rapid increase at low driving voltage (V_d) ranging from −0.25 to 0.25 V. Shao and his co-workers also observed the sigmoid responses in a bipolar transistor by modifying different molecules carrying different charges on the surface of a theta capillary.[30] It is interesting to note that these steep responses in a very narrow range and their related switch functions in signal transmission have been applied into artificial neural network and machine learning.[31−33] In the case of V_d < 0 and V_B > 0, the responses of I_C are expected to be in a corresponding active mode of BJT because I_C is dependent on V_B and one of bipolar junction is at off state. Saturation mode could be found in the case of V_d > 0 and V_B = −0.5 V or −0.2 V, which could generate the highest current (I_C, Figure 2b) except for the breakdown mode in Figure 2c with the corresponding currents independent of V_B. When the applied V_d is smaller than 0 V and V_B remains at −0.5 V or −0.2 V, the operating mode should be equal to the cutoff mode with tiny current. However, our experimental results demonstrate that the PNP nBJT still shows finite current (Figure 2b). This could be attributed to the larger diameters of the PET nanochannel,

https://doi.org/10.1021/acs.nanolett.2c00312
Nano Lett. 2022, 22, 3678−3684

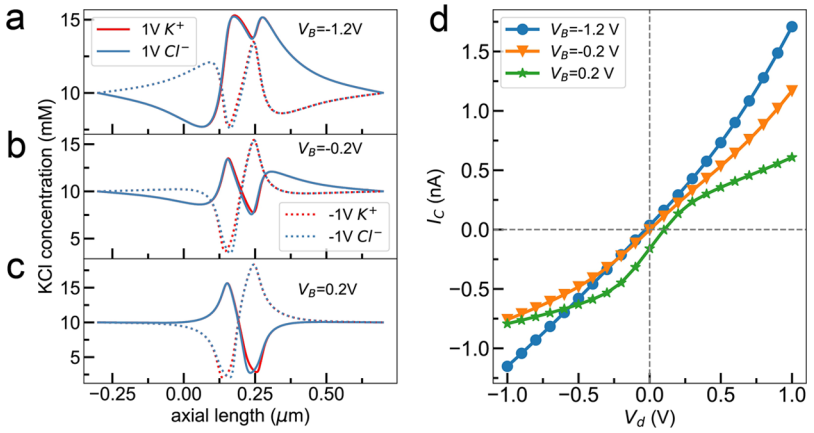

Figure 3. Concentration profiles along the nanochannel of different PNP nBJTs and corresponding current responses. (a–c) Concentration profiles of K^+ and Cl^- along the nanochannel of PNP nBJTs with base voltages of −1.2, −0.2, and 0.2 V, respectively. Red and blue solid lines represent the concentration distributions of K^+ and Cl^- along the nanochannel with 1.0 V driving voltage, respectively. Red and blue dotted lines represent the concentration distributions of K^+ and Cl^- along the nanochannel with −1.0 V driving voltage, respectively. (d) Corresponding current responses with base voltages of −1.2 (blue solid line), −0.2 (orange solid line), and 0.2 V (green solid line), respectively.

which results in a weak ion depletion region limiting the ion transportation. I_C displays a quasi-linear relationship when the base voltage (V_B) is below −0.5 V (Figure 2c). Under this circumstance, the PANI layer at its reducing state does not carry any charges. The whole PNP nBJT carries negative charges since the excessive negative base voltage makes the PANI membrane carrying with negative charges, leading to the quasi-linear response in current with V_d. In this region, the device shows a breakdown mode.

We then performed theoretical simulations that were used to further understand the above experimental results. Figure 2d–f presents the simulated curves of I_C under different V_B. When the applied V_B is set from 0 to 0.4 V (Figure 2d), the I–V curves display clear "S" shapes. However, the sigmoid curve could not be observed at 0.4 V (V_B) because of a larger leakage current in I_B generated by the electrical conductivity of PANI. The ionic current dramatically is increased when V_d is increased from −0.25 to 0.25 V, whereas it is slowly increased when V_d is increased from −1.0 to −0.25 V and from 0.25 to 1 V. With the increase of V_B from −0.5 to −0.2 V (Figure 2e), the I_C–V relationship is changed to partial rectification. These simulated results are in good agreement with the experimental ones, demonstrating that various I_C–V responses can be implemented simply by varying V_B. Figure 2f shows a quasi-linear relationship between the ionic currents and the driving voltage with V_B ranging from −1.5 to −1.2 V. These results suggest that PNP nBJT might become useful nanofluidic components in fabrication of smart devices by actively responding to the environments.

Since a highly concentrated electrolyte can screen the electrostatic interaction, the ionic current at different base voltages only displays linear and weak rectification behaviors in 100 mM KCl solution (Figure S6).

In addition, we applied cyclic voltammetry (CV) to investigate the redox lifetime of PANI coating on PET membrane in 1 M KCl solution with pH of 5. During the experiment, the voltage scan range was set from −0.2 to 0.9 V with a scan rate of 0.1 V/s. We recorded 200 times continuous cycles of the oxidation and reduction processes of the PANI membrane. As shown in Figure S7, the oxidation and reduction peaks continuously appear within the 200th redox cycles. However, the corresponding peak currents gradually decrease, which could be attributed to possibly a partial fall off of the PANI coating layer from the PET membrane because of the intercalation/deintercalation processes of ions under the electric field.[34] The results show that the PNP nBJT could last about 100 redox cycles. To improve the lifetime of this device, we are going to adopt dopants to decrease ions intercalation.

The profiles of ion concentrations along the PNP nBJT were calculated by simulation to understand the ionic current. Figure 3a shows that an application of V_B of −1.2 V brings about a significant enrichment of K^+ and Cl^- in the PNP nBJT without regard to the driving voltage V_d, showing a quasi-linear relationship between I_C and V_d (Figure 3d, blue solid line with circles). An increase of the base voltage to −0.2 V (Figure 3b) results in enrichment and depletion of K^+ and Cl^- concentration along the PNP nBJT at driving voltages ranging from 1.0 to −1.0 V, leading to rectifying effects of I_C (Figure 3d, orange solid line with downward triangles). When the base voltage is further increased to 0.2 V, the profiles of K^+ and Cl^- concentration at driving voltages of ±1 V exhibit a central-symmetry distribution (Figure 3c). At 1.0 V of V_d, enrichment of K^+ and Cl^- regions occurs along the nanochannel from 0 to 0.25 μm, and the depletion happens along the nanochannel from 0.25 to 0.4 μm. At −1.0 V of V_d, the locations of the enrichment and depletion regions are exchanged as compared with the results at 1.0 V of V_d. These results suggest that the central-symmetric profiles bring about the appearance of sigmoid relationship between I_C and V_d (Figure 3d, green solid line with asterisks). As shown in Figure S8, the concentration of ions increases rapidly with the driving voltage and then tends to be saturated at higher driving voltages, thus, sigmoid relationship between I_C and V_d is obtained. Additionally, because the PET nanochannel and oxidized PANI carry negative and positive charges, respectively, excess amounts of K^+ or Cl^- ions are required to balance the corresponding surface charges to meet the electroneutral conditions. As a result, it is unlikely for profiles of K^+ and Cl^- to overlap completely under each operating voltage.

The PANI layer thickness has also an effect on the ion transport behavior of the PNP nBJTs. When the PANI layer thickness decreases from 5 to 1 μm, the relationship between I_C and V changes from sigmoid to quasi-linear at 0.2 V of V_B

https://doi.org/10.1021/acs.nanolett.2c00312
Nano Lett. 2022, 22, 3678−3684

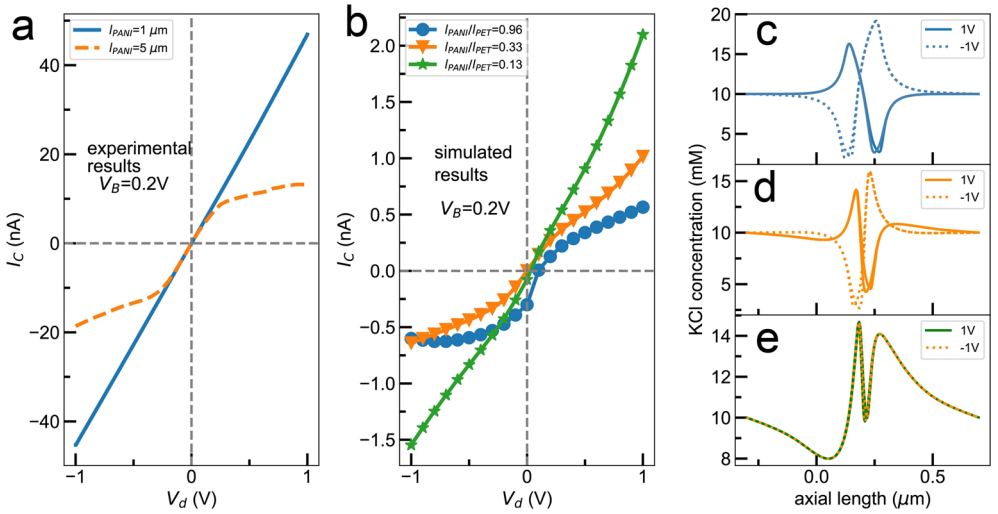

Figure 4. Effect of PANI layer thickness on ion transport. (a) Measured $I-V$ curves of the PNP nBJTs with different thicknesses of PANI layer in response to 0.2 V base voltage. (b) Simulated I_C-V curves of the PNP nBJTs with different thickness ratios (0.96, 0.33, and 0.13) of PANI to PET. Base voltage: 0.2 V; (c–e) profiles of ion concentrations along PNP nBJTs with different thicknesses of PANI layer in PNP nBJT.

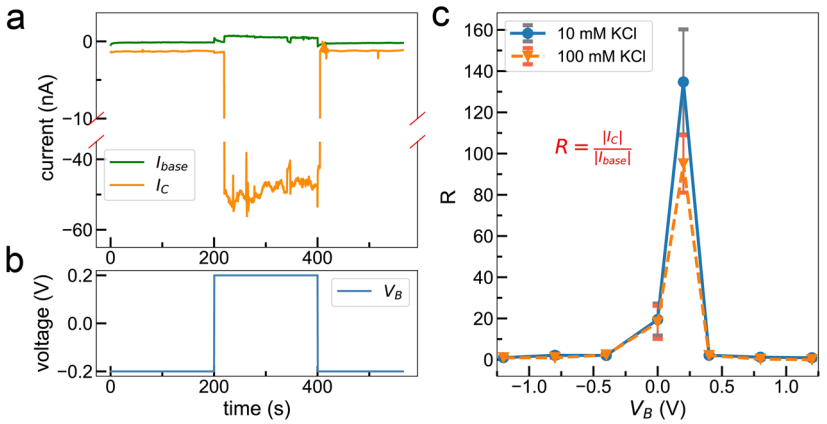

Figure 5. Transient current response and amplification effects of a PNP nBJT. (a) Transient current responses to a voltage step from −0.2 to 0.2 V in V_B. (b) I_C of PNP nBJT at the driven voltage of −1 V correlates with I_{base}. (c) Current gain ($R = |I_C/I_{base}|$) of PNP nBJT as a function of V_B in 10 mM and 100 mM KCl, respectively. The error bars are calculated from 5 tests of every applied V_B.

(Figure 4a). This change in $I-V$ relationship is also supported by the simulated results as shown in Figure 4b. The simulated results also show that the PANI layer thickness affects the profiles of ion concentration distributions in PNP nBJT. When the PANI layer thickness is approximately equal to the PET membrane, symmetric concentration profiles for both cations and anions are obtained at V_d of 1.0 V and −1.0 V, respectively, thus the ionic currents at the driving voltages of ±1 V are similar (Figure 4c). When the PANI layer thickness is decreased to 33% of the PET membrane, the ionic accumulation and depletion regions are close to each other along the symmetric axis (Figure 4d). With further decrease of the PANI layer thickness to 13% of the PET membrane, the profiles of ion concentrations at driving voltages of −1 and 1 V overlap each other (Figure 4e), leading to linear responses of the ionic currents. The whole positive charges in PANI layer decreases with the decrease of its thickness. When the PANI layer is thinner than 13% of the PET membrane, the positive charges in PANI are not enough to modulate the ion transport in the PNP nBJT, resulting in a quasi-linear I_C-V relationship. These simulation results imply that the PANI layer thickness has a great effect on the ion transport behavior of the PNP nBJTs and should be considered for fabrication of PNP nBJTs with defined functions.

The transient switch from cutoff mode to active mode was investigated by applying a step voltage (V_B) from −0.2 to 0.2 V at a driving voltage (V_d) of −1 V. When the PNP nBJT is switched from the cutoff mode (V_B= −0.2 V) to the active mode (V_B = 0.2 V), I_C experiences a rapid growth after a delay of 20 s (Figures 5a,b). Compared with electrons and holes in semiconductor, the slow transport rate of ions in solution and in membrane increases the time of transient current responses in our device. It is well-known that traditional transistors (either PNP or NPN) could be used as current amplifiers in circuits. Figure 5c illustrates that the current amplification of our PNP nBJT can be modulated by the base current induced by varied V_B. As shown in Figure 5c, the highest current gain ($R = |I_C/I_{base}|$) in PNP nBJT could reach about 134.5 in 10 mM KCl. It is interesting to note that the current gain only drops to about 95 in the solution of 100 mM KCl, indicating the impacts of the electrolyte concentrations. The decreased current gain could be ascribed to the decreased thickness of the electric double layer at higher ionic strength. It needs to be emphasized that even in the solution of 100 mM KCl, the

https://doi.org/10.1021/acs.nanolett.2c00312
Nano Lett. 2022, 22, 3678−3684

current gain is still much higher than those reported previously.[23,24,35] The results demonstrate that our PNP nBJT can amplify the ionic signals with the same mechanisms as in traditional electronic transistors.

When V_B is set at −0.2 V, the PANI layer will be converted to its reducing state and carries nearly zero charge. The nBJT becomes the connection of two bipolar nanofluidic channels. Thus, the current gain rapidly decreases to a very low value. With the further decrease of V_B to −1.20 V, the current gain decreases to be 1 (Figure 5c). These phenomena are also observed when the applied V_B is higher, that is, 0.2 V.

CONCLUSION

In summary, PNP nBJTs with tunable current gain have been fabricated by sandwiching a PANI membrane between two PET membranes. Experimental results and simulations indicate that the PNP nBJTs can perform similar functions of ionic rectification and signal amplification as in the case of traditional transistors. These observed functions can be explained by the simulated concentration profiles at different conditions. The present PNP nBJTs can reach relatively high current gain of over one hundred folds at very low base voltage of 0.2 V. Since chemically prepared PANI contains a simultaneously reduced and oxidized state,[36] it results in conductivity of PANI. Pure reduced state or oxidized state is an insulator. However, electrochemical method hardly converts prepared PANI into an oxidized or reduced state thoroughly unless applying strong oxidant or reductant. Therefore, the leakage current at the PANI layer would increase the quantity of I_{base}, especially when applied high V_B on PANI layer, which reduced the current amplification ratio. In the subsequent research, we would apply a strong oxidant to help convert PANI into an oxidized state fully for improving current amplified effect of PNP nBJT. This study provides an approach to the design of nanofluidic devices with logical control functions for ultrasensitive analysis and mimics the information transmission of biological systems.

ASSOCIATED CONTENT

Supporting Information

The Supporting Information is available free of charge at https://pubs.acs.org/doi/10.1021/acs.nanolett.2c00312.

Experimental section, numerical models, and schematic illustration of fabrication of PNP nanofluidic transistor (PDF)

AUTHOR INFORMATION

Corresponding Authors

Xiao-Lei Huo − *School of Public Health, Nantong University, Nantong, Jiangsu 226019, China*; Email: hxl362349@ntu.edu.cn

Zeng-Qiang Wu − *School of Public Health, Nantong University, Nantong, Jiangsu 226019, China*; orcid.org/0000-0001-8210-453X; Email: zqwu@ntu.edu.cn

Xing-Hua Xia − *State Key Laboratory of Analytical Chemistry for Life Science, School of Chemistry and Chemical Engineering, Nanjing University, Nanjing, Jiangsu 210023, China*; orcid.org/0000-0001-9831-4048; Email: xhxia@nju.edu.cn

Authors

Yu-Lin Hu − *School of Public Health and School of Chemistry and Chemical Engineering, Nantong University, Nantong, Jiangsu 226019, China*

Yu Hua − *School of Public Health, Nantong University, Nantong, Jiangsu 226019, China*

Zhong-Qin Pan − *School of Public Health, Nantong University, Nantong, Jiangsu 226019, China*

Jia-Han Qian − *School of Chemistry and Chemical Engineering, Nantong University, Nantong, Jiangsu 226019, China*

Xiao-Yang Yu − *School of Chemistry and Chemical Engineering, Nantong University, Nantong, Jiangsu 226019, China*

Ning Bao − *School of Public Health, Nantong University, Nantong, Jiangsu 226019, China*

Complete contact information is available at: https://pubs.acs.org/10.1021/acs.nanolett.2c00312

Author Contributions

‖Y.-L.H. and Y.H. contributed equally.

Notes

The authors declare no competing financial interest.

ACKNOWLEDGMENTS

This work was supported by grants from the National Natural Science Foundation of China (21775066, 21974058, and 22074061). We also gratefully acknowledge the service of scanning electron microscope provided by Analysis & Testing center of Nantong University.

REFERENCES

(1) Wang, X.; Wilkinson, M. D.; Lin, X.; Ren, R.; Willison, K. R.; Ivanov, A. P.; Baum, J.; Edel, J. B. Single-molecule nanopore sensing of actin dynamics and drug binding. *Chem. Sci.* **2020**, *11*, 970−979.

(2) Im, J.; Lindsay, S.; Wang, X.; Zhang, P. Single Molecule Identification and Quantification of Glycosaminoglycans Using Solid-State Nanopores. *ACS Nano* **2019**, *13*, 6308−6318.

(3) He, Y.; Gillespie, D.; Boda, D.; Vlassiouk, I.; Eisenberg, R. S.; Siwy, Z. S. Tuning Transport Properties of Nanofluidic Devices with Local Charge Inversion. *J. Am. Chem. Soc.* **2009**, *131*, 5194−5202.

(4) Ali, M.; Ramirez, P.; Mafe, S.; Neumann, R.; Ensinger, W. A pH-Tunable Nanofluidic Diode with a Broad Range of Rectifying Properties. *ACS Nano* **2009**, *3*, 603−608.

(5) Schoch, R. B.; Han, J.; Renaud, P. Transport phenomena in nanofluidics. *Rev. Mod. Phys.* **2008**, *80*, 839−883.

(6) Wang, M.; Hou, Y.; Yu, L.; Hou, X. Anomalies of Ionic/Molecular Transport in Nano and Sub-Nano Confinement. *Nano Lett.* **2020**, *20*, 6937−6946.

(7) Li, J.; Stein, D.; McMullan, C.; Branton, D.; Aziz, M. J.; Golovchenko, J. A. Ion-beam sculpting at nanometre length scales. *Nature* **2001**, *412*, 166−169.

(8) Wei, C.; Bard, A. J.; Kapui, I.; Nagy, G.; Toth, K. Scanning electrochemical microscopy. 32. Gallium ultramicroelectrodes and their application in ion-selective probes. *Anal. Chem.* **1996**, *68*, 2651−2655.

(9) Li, Z.-Q.; Wang, Y.; Wu, Z.-Q.; Wu, M.-Y.; Xia, X.-H. Bioinspired Multivalent Ion Responsive Nanopore with Ultrahigh Ion Current Rectification. *J. Phys. Chem. C* **2019**, *123*, 13687−13692.

(10) Daiguji, H.; Oka, Y.; Shirono, K. Nanofluidic diode and bipolar transistor. *Nano Lett.* **2005**, *5*, 2274−2280.

(11) Cheng, L.-J.; Guo, L. J. Rectified ion transport through concentration gradient in homogeneous silica nanochannels. *Nano Lett.* **2007**, *7*, 3165−3171.

(12) Wu, Z.-Q.; Li, Z.-Q.; Wang, Y.; Xia, X.-H. Regulating Ion Transport in a Nanochannel with Tandem and Parallel Structures via Concentration Polarization. *J. Phys. Chem. Lett.* **2020**, *11*, 524−529.
(13) Ali, M.; Ramirez, P.; Nasir, S.; Cervera, J.; Mafe, S.; Ensinger, W. Ionic circuitry with nanofluidic diodes. *Soft Matter* **2019**, *15*, 9682−9689.
(14) Gomez, V.; Ramirez, P.; Cervera, J.; Ali, M.; Nasir, S.; Ensinger, W.; Mafe, S. Concatenated logic functions using nanofluidic diodes with all-electrical inputs and outputs. *Electrochem. Commun.* **2018**, *88*, 52−56.
(15) Ramirez, P.; Gomez, V.; Verdia-Baguena, C.; Nasir, S.; Ali, M.; Ensinger, W.; Mafe, S. Designing voltage multipliers with nanofluidic diodes immersed in aqueous salt solutions. *Phys. Chem. Chem. Phys.* **2016**, *18*, 3995−3999.
(16) Cervera, J.; Ramirez, P.; Gomez, V.; Nasir, S.; Ali, M.; Ensinger, W.; Stroeve, P.; Mafe, S. Multipore membranes with nanofluidic diodes allowing multifunctional rectification and logical responses. *Appl. Phys. Lett.* **2016**, *108*, 253701.
(17) Ramirez, P.; Cervera, J.; Gomez, V.; Ali, M.; Nasir, S.; Ensinger, W.; Mafe, S. Optimizing Energy Transduction of Fluctuating Signals with Nanofluidic Diodes and Load Capacitors. *Small* **2018**, *14*, 1702252.
(18) Alcaraz, A.; Ramirez, P.; Garcia-Gimenez, E.; Lopez, M. L.; Andrio, A.; Aguilella, V. M. A pH-tunable nanofluidic diode: Electrochemical rectification in a reconstituted single ion channel. *J. Phys. Chem. B* **2006**, *110*, 21205−21209.
(19) Macrae, M. X.; Blake, S.; Mayer, M.; Yang, J. Nanoscale Ionic Diodes with Tunable and Switchable Rectifying Behavior. *J. Am. Chem. Soc.* **2010**, *132*, 1766−1767.
(20) Yameen, B.; Ali, M.; Neumann, R.; Ensinger, W.; Knoll, W.; Azzaroni, O. Proton-regulated rectified ionic transport through solid-state conical nanopores modified with phosphate-bearing polymer brushes. *Chem. Commun.* **2010**, *46*, 1908−1910.
(21) Guan, W.; Fan, R.; Reed, M. A. Field-effect reconfigurable nanofluidic ionic diodes. *Nat. Commun.* **2011**, *2*, 506.
(22) Ren, R.; Zhang, Y.; Nadappuram, B. P.; Akpinar, B.; Klenerman, D.; Ivanov, A. P.; Edel, J. B.; Korchev, Y. Nanopore extended field-effect transistor for selective single-molecule biosensing. *Nat. Commun.* **2017**, *8*, 586.
(23) Tybrandt, K.; Larsson, K. C.; Richter-Dahlfors, A.; Berggren, M. Ion bipolar junction transistors. *Proc. Natl. Acad. Sci. USA* **2010**, *107*, 9929−9932.
(24) Sun, G.; Senapati, S.; Chang, H.-C. High-flux ionic diodes, ionic transistors and ionic amplifiers based on external ion concentration polarization by an ion exchange membrane: a new scalable ionic circuit platform. *Lab Chip* **2016**, *16*, 1171−1177.
(25) Perez-Mitta, G.; Marmisolle, W. A.; Trautmann, C.; Toimil-Molares, M. E.; Azzaroni, O. Nanofluidic Diodes with Dynamic Rectification Properties Stemming from Reversible Electrochemical Conversions in Conducting Polymers. *J. Am. Chem. Soc.* **2015**, *137*, 15382−15385.
(26) Hao, Z.; Zhou, T.; Xiao, T.; Gong, H.; Zhang, Q.; Wang, H.; Zhai, J. Electrochromic Nanochannels for Visual Nanofluidic Manipulation in Integrated Ionic Circuits. *ACS Appl. Mater. Interfaces* **2020**, *12*, 57314−57321.
(27) Wen, L.; Jiang, L. Construction of biomimetic smart nanochannels for confined water. *Natl. Sci. Rev.* **2014**, *1*, 144−156.
(28) Dauginet, L.; Duwez, A. S.; Legras, R.; Demoustier-Champagne, S. Surface Modification of Polycarbonate and Poly(ethylene terephthalate) Films and Membranes by Polyelectrolyte Deposition. *Langmuir* **2001**, *17*, 3952−3957.
(29) Chun, H.; Chung, T. D. Iontronics. *Annual Review of Analytical Chemistry* **2015**, *8*, 441−462.
(30) Zhang, S.; Yin, X.; Li, M.; Zhang, X.; Zhang, X.; Qin, X.; Zhu, Z.; Yang, S.; Shao, Y. Ionic Current Behaviors of Dual Nano- and Micropipettes. *Anal. Chem.* **2018**, *90*, 8592−8599.
(31) Gibbs, M. N.; MacKay, D. J. C. Variational Gaussian process classifiers. *IEEE Trans. Neural Networks* **2000**, *11*, 1458−1464.
(32) Leibowitz, N.; Baum, B.; Enden, G.; Karniel, A. The exponential learning equation as a function of successful trials results in sigmoid performance. *J. Math. Psychol.* **2010**, *54*, 338−340.
(33) Lewicki, G.; Marino, G. Approximation of functions of finite variation by superpositions of a sigmoidal function. *Appl. Math. Lett.* **2004**, *17*, 1147−1152.
(34) Feng, X.-M.; Li, R.-M.; Ma, Y.-W.; Chen, R.-F.; Shi, N.-E.; Fan, Q.-L.; Huang, W. One-Step Electrochemical Synthesis of Graphene/Polyaniline Composite Film and Its Applications. *Adv. Funct. Mater.* **2011**, *21*, 2989−2996.
(35) Lucas, R. A.; Lin, C.-Y.; Baker, L. A.; Siwy, Z. S. Ionic amplifying circuits inspired by electronics and biology. *Nat. Commun.* **2020**, *11*, 1568.
(36) Wei, Y.; Hsueh, K. F.; Jang, G.-W. A study of leucoemeraldine and the effect of redox reactions on the molecular weight of chemically prepared polyaniline. *Macromolecules* **1994**, *27*, 518−525.

https://doi.org/10.1021/acs.nanolett.2c00312
Nano Lett. 2022, 22, 3678−3684